S. Yliniemi, J. Albert, and S. Honkanen, A study of silver-film ion-exchanged glass waveguides in phosphate glass, in Optical Components and Materials IV, Shibin Jiang and Michel J. F. Digonnet, eds., Proceedings of SPIE 6469, 64690Y (2007), 8 pages.

A study of silver-film ion-exchanged glass waveguides in phosphate glass

Sanna Yliniemi[a], Jacques Albert[b], and Seppo Honkanen[c]

[a]Helsinki University of Technology, Optoelectronics laboratory, Tietotie 3, P.O.Box 3500, Espoo, FIN-02150 HUT, Finland;
[b]Carleton University, Department of Electronics, 1125 Colonel By Drive, Ottawa, Ontario, Canada K1S 5B6;
[c]University of Arizona, College of Optical Sciences, Meinel Building, 1630 East University Boulevard, Tucson, Arizona 85721, USA

ABSTRACT

In this work, properties of Ag thin-film ion exchange in Schott IOG-1 phosphate glass has been studied. Emphasis has been put on finding the proper diffusion parameters (self-diffusion coefficient for Ag^+ ions and the mobility ratio between the participating ions) at process temperatures of 90°C and 230°C. In order to extract the diffusion parameters a following procedure was utilized: An ion-exchanged slab waveguide was fabricated using the same process conditions as in the case of a two-dimensional waveguide fabrication. After slab waveguide fabrication, the effective refractive indices of the propagating modes were measured by prism coupling. Thereafter, a smooth refractive index profile was constructed by improved inverse Wentzel-Kramers-Brillouin method. This refractive index profile was compared with the Ag^+ ion concentration profile calculated from the diffusion equation by Crank-Nicolson method. The self-diffusion coefficient for Ag^+ ions and the ratio of the self-diffusion coefficients of Ag^+ and Na^+ ions were varied until convergence between the refractive index profile and the concentration profile was found. Using the diffusion parameters obtained from these experiments, two-dimensional waveguide mode profiles were calculated by finite difference method. These theoretically obtained mode profiles were compared with the measured mode profiles with different mask opening widths.

1. INTRODUCTION

Silver-sodium thin-film ion exchange is a powerful method for fabricating waveguides for integrated optics components. Being a dry process, this $Ag^+ - Na^+$ ion exchange is particularly well suited for fabricating components in phosphate glass that is known to have chemical durability issues when used with molten salt processes. In spite of this, phosphate glass is an attractive choice for waveguide lasers due to its high solubility of rare earth ions enabling high gain values in short cavity lengths. Quite recently, many waveguide lasers have been realized in phosphate glass, either using $Ag^+ - Na^+$ or $K^+ - Na^+$ ion exchange.[1–4] Compared with $K^+ - Na^+$ ion exchange, $Ag^+ - Na^+$ ion exchange produces higher maximum refractive index change in the glass resulting in smaller mode profile dimensions and wider wavelength tunability in waveguide laser arrays that use a common feedback grating.

Several key process parameters, e. g., self-diffusion coefficient D_{Ag}, the ratio of the self-diffusion coefficients of Ag^+ and Na^+ ions (also called mobility M), and diffusion length, can be deduced from the combined information of refractive index and concentration profiles. Knowledge of these parameters and the maximum refractive index change Δn_{max} obtained from the refractive index profile analysis enables us to find out the light guiding properties in waveguides and, therefore, to control these properties by choosing proper process conditions. Parameter extraction through comparing the theoretically calculated concentration profiles with the measured ones from one dimensional slab waveguides was performed by Honkanen *et al.*[5] These experiments were carried out in borosilicate glass (Corning 0211) and at temperatures well above (> 299°C) the postbake temperature of 230°C used in this study. Therefore, the diffusion parameters extracted from these experiments are not applicable as

Further author information: (Send correspondence to S. Yliniemi)
S. Yliniemi: E-mail: sanna.yliniemi@tkk.fi, Telephone: +358 9 451 3129

Optical Components and Materials IV, edited by Shibin Jiang, Michel J. F. Digonnet,
Proc. of SPIE Vol. 6469, 64690Y, (2007) · 0277-786X/07/$18 · doi: 10.1117/12.723993

such at process conditions used to fabricate two-dimensional channel waveguides in phosphate glass. Self-diffusion coefficient is known to have a strong dependence on temperature; it inceases exponentially with the inverse of temperature.[6] In this work, we adopt a similar approach as Honkanen *et al.* to define the self-diffusion constant and the ratio of the self-diffusion coefficients of Ag^+ and Na^+ ions at ion exchange and postbake temperatures, and we then proceed to calculate the theoretical mode profiles for waveguides with varying mask opening widths at signal (1535 nm) and pump (980 nm) wavelengths, and finally compare the results with the measured mode profiles. The signal wavelength was chosen to be equal to 1535 nm since the gain maximum of erbium doped glass occurs at this wavelength, and therefore provides the lowest threshold and the highest output power available from Er^{3+}-doped glass lasers. However, the mode profile dimensions are approximately the same within the whole C-band.

2. THEORETICAL BACKGROUND

Theory of the waveguide fabrication by $Ag^+ - Na^+$ thin film ion exchange has been presented in depth in Refs. 7–9. In electric field assisted binary ion exchange, the effect of both thermal diffusion and ion migration due to the force $q\mathbf{E}$ caused by the driving electric field must be taken into account. The time evolution of the concentration profile can be described by the equation[9]

$$\frac{\partial C}{\partial t} = \frac{D\nabla^2 C}{C(M-1)+1} - \frac{D(M-1)(\nabla C)^2 + M\mathbf{J}_0 \cdot \nabla \mathrm{C}}{[C(M-1)+1]^2}, \tag{1}$$

where D is the diffusion coefficient of Ag^+ ions, M is the ratio of the self-diffusion coefficients of the ions participating in the ion exchange, or D_{Ag}/D_{Na}, C is the normalized Ag^+ ion concentration, and $\mathbf{J}_0$ represents the normalized ion flux due to the applied electric field.

The electric field assisted diffusion equation (1) must be solved with appropriate boundary conditions. Thin film $Ag^+ - Na^+$ ion exchange can be considered as an electrolysis process in which positively charged Ag^+ ions drift from a solid electrolyte (silver anode) towards the silver cathode.[7,9] The ion flux $\mathbf{J}_{\mathrm{Ag}}$ is perpendicular to the surface chosen here to be along y-direction. The surface boundary condition is given therefore by

$$\mathbf{J}_{\mathrm{Ag}} = \mathbf{J}_0. \tag{2}$$

The Ag^+ ion flux on other surfaces is zero. The normalized ion flux $\mathbf{J}$ can be solved if we combine both the effect of thermal ion diffusion and the ion migration due to the applied field, and can be written as[9]

$$\mathbf{J} = \frac{-\mathrm{D}\nabla \mathrm{C} + \mathrm{MC}\mathbf{J}_0}{\mathrm{C(M-1)+1}}. \tag{3}$$

By substituting Eq. (2) into Eq. (3), the boundary conditions for thin film $Ag^+ - Na^+$ ion exchange can be presented in a more useful form as

$$\frac{\partial C}{\partial y} = \begin{cases} J_0\left(C_{Ag}-1\right)/D & \text{surface in contact with a silver thin film source} \\ 0 & \text{other surfaces} \end{cases}.$$

2.1. Solving the 1-dimensional diffusion equation with the Crank-Nicolson method

Since our method involves calculation of the Ag^+ ion concentration profile in a slab waveguide, it is enough to solve the one-dimensional diffusion equation

$$\frac{\partial C}{\partial t} = \frac{D\frac{\partial^2 C}{\partial x^2}}{C(M-1)+1} - \frac{D(M-1)\left(\frac{\partial C}{\partial x}\right)^2}{\left[C_i^s(M-1)+1\right]^2} + \frac{M\mathbf{J}_0 \cdot \frac{\partial \mathrm{C}}{\partial \mathrm{x}}}{[C(M-1)+1]^2} \tag{4}$$

with appropriate boundary conditions. Equation (4) is a one-dimensional time-dependent parabolic partial-differential equation which can be solved efficiently by Crank-Nicolson method.[10] In the following we show how the concentration profile at advanced moment C^{s+1} can be determined by solving a matrix equation where the knowledge of the concentration profile values at different spatial nodes i at the moment s are preserved in

a tridiagonal matrix Ξ and the inhomogeneous vector Θ. The resulting tridiagonal system can be solved by Gaussian elimination.[11]

The partial derivatives in Eq. (4) can be expressed in finite difference form as

$$\frac{\partial C}{\partial t} \approx \frac{C_i^{s+1} - C_i^s}{\delta t} \tag{5}$$

for the temporal derivative, and

$$\frac{\partial C}{\partial x} \approx \frac{C_{i+1}^s - C_{i-1}^s}{2\delta x} \tag{6}$$

and

$$\frac{\partial^2 C}{\partial x^2} \approx \frac{C_{i+1}^s - 2C_i^s + C_{i-1}^s}{(\delta x)^2} \tag{7}$$

for the spatial derivatives. Superscripts describe the value of the concentration profile C at moments s and $s+1$. The timestep is equal to δt. The value of C at the moment s is known while the value of C at the advanced moment $s+1$ is to be calculated based on the data at earlier moments s. Subscripts denote the spatial node indices. The spatial step is equal to δx. By inserting the partial derivatives (5)-(7) we obtain

$$\frac{C_i^{s+1} - C_i^s}{\delta t} = \frac{D}{C_i^s(M-1)+1}\frac{1}{2}\left[\frac{C_{i+1}^s - 2C_i^s + C_{i-1}^s}{(\delta x)^2} + \frac{C_{i+1}^{s+1} - 2C_i^{s+1} + C_{i-1}^{s+1}}{(\delta x)^2}\right] \tag{8}$$

$$- \frac{D(M-1)}{[C_i^s(M-1)+1]^2}\left[\frac{C_{i+1}^s - C_{i-1}^s}{2\delta x}\cdot\frac{C_{i+1}^{s+1} - C_{i-1}^{s+1}}{2\delta x}\right] \tag{9}$$

$$- \frac{M\mathbf{J}_0}{[C_i^s(M-1)+1]^2}\frac{1}{2}\left[\frac{C_{i+1}^s - C_{i-1}^s}{2\delta x} + \frac{C_{i+1}^{s+1} - C_{i-1}^{s+1}}{2\delta x}\right]. \tag{10}$$

By arranging the terms and by multiplying both sides by $2\delta x(C_i^s(M-1)+1)$, the above equation can be obtained into a more convenient form

$$\chi_{-1}C_{i-1}^{s+1} + \chi_0 C_i^{s+1} + \chi_{+1}C_{i+1}^{s+1} = \theta, \tag{11}$$

where

$$\chi_{-1} = \frac{D}{\delta x} + \frac{1}{2\delta x}\frac{D(M-1)(C_{i+1}^s - C_{i-1}^s)}{C_i^s(M-1)+1} + \frac{J_0 M}{2(C_i^s(M-1)+1)}, \tag{12}$$

$$\chi_0 = \frac{-2D}{\delta x} - \frac{2\delta x(C_i^s(M-1)+1)}{\delta t}, \tag{13}$$

$$\chi_{+1} = \frac{D}{\delta x} - \frac{1}{2\delta x}\frac{D(M-1)(C_{i+1}^s - C_{i-1}^s)}{C_i^s(M-1)+1} - \frac{J_0 M}{2(C_i^s(M-1)+1)}, \tag{14}$$

and

$$\theta = \frac{-2\delta x(C_i^s(M-1)+1)C_i^s}{\delta t} - \frac{D(C_{i+1}^s - 2C_i^s + C_{i-1}^s)}{\delta x} + \frac{MJ_0(C_{i+1}^s - C_{i-1}^s)}{2(C_i^s(M-1)+1)}. \tag{15}$$

The concentration profile C at advanced time can be therefore determined by solving the matrix equation

$$\Xi\mathbf{c} = \Theta, \tag{16}$$

where Θ is a vector of the inhomogeneous terms θ, $\mathbf{c}$ contains the desired concentration values, and

$$\Xi = \begin{bmatrix} \chi_0 & \chi_{+1} & 0 & 0 & \dots & 0 \\ \chi_{-1} & \ddots & \ddots & & & \vdots \\ 0 & \ddots & \ddots & \ddots & & \\ 0 & & \ddots & \ddots & \ddots & \\ \vdots & & & \ddots & \ddots & \ddots \\ 0 & \dots & & & \ddots & \ddots \end{bmatrix}.$$

2.2. Refractive index profile by inverse Wentzel-Kramers-Brillouin method

Determining the refractive index profile (refractive index vs. depth) from the measured mode index data is an inverse problem utilizing Wentzel-Kramers-Brillouin (WKB) approximation widely deployed in quantum mechanics to calculate the energy eigenstates of electrons in a potential well.[12,13] WKB approximation is applicable in cases where the potential, $V(x)$, is a slowly varying function of x. The analogy to the guided modes in a diffused waveguide is obvious at this point: the graded refractive index profile of an ion-exchanged slab waveguide represents the slowly varying potential and the guided modes measured by prism coupling method correspond to the bound states of the electron.[14] The characteristic equation for the mth order mode in a slab waveguide is given by

$$k\int_0^{x_t(m)}\left[n^2(x)-N^2(m)\right]^{1/2}dx = mx+\phi_a+\phi_s, \tag{17}$$

where k is the wavevector in free space, $n(x)$ is the refractive index profile, $N(x)$ corresponds to the effective refractive index of the mth mode. m is the mode index number (in case of real physical modes m is an integer), ϕ_a is the phase change at the waveguide-air interface, and ϕ_s is the phase change at the turning point x_t.

The phase change at the surface-waveguide interface can be derived from Fresnel's equations of reflection for s- and p-polatizations and is given by[14,15]

$$2\phi_a = 2\arctan\left\{r_a\left[\frac{N^2(m)-n_a^2}{n_0^2-N^2(m)}\right]^{1/2}\right\}, \tag{18}$$

where n_a is the refractive index of air, parameter r_a is 1 for quasi TE-polarization and $(n_0/n_a)^2$ for quasi TM-polarization, and n_0 is the maximum refractive index reached close to the waveguide-air interface. The phase shift at the turning point ϕ_s can be derived from the boundary conditions in the WKB approximation and corresponds to a value of $\pi/4$.[12,13]

In 1984, Chiang[16] proposed a novel solution to the inverse WKB problem in diffused waveguides. In this approach, an advantage is taken of virtual modes corresponding to non-integer mode numbers m. In this way, a smooth index profile can be constructed, smoothness depending on the number of mode indices in contrast to the earlier methods in which the index profile consists only as many points as there are real modes propagating in the waveguide.[16] In Chiang's approach, the measured refractive indices are first arranged in increasing order of the mode index number m_i. By fitting a suitable continuous function to the measured refractive index values, the estimates for the peak index n_0 at m_0 and the refractive indices for the virtual modes at m_i are obtained. The mode index number corresponding to the maximum refractive index at $x=0$ is obtained from Eq. (17) by noting that the left hand side of the equation has to be zero ($n_0 = n(0) = N(m_0)$) and by substituting the value of $\pi/2$ for the phase change ϕ_a (calculated from Eq. (18)). We therefore conclude that the virtual mode number m_0 for the peak refractive index n_0 has to be -0.75. In Chiang's approach, the left hand side integral in Eq. (17) is replaced by a sum

$$\begin{aligned} I &\cong k\left\{\left(\bar{N}_1^2-N_i^2\right)^{1/2}(x_1-x_0)+\left(\bar{N}_2^2-N_i^2\right)^{1/2}(x_2-x_1)+\ldots+\left(\bar{N}_i^2-N_i^2\right)^{1/2}(x_i-x_{i-1})\right\} && (19)\\ &= k\left\{x_i\left(\bar{N}_i^2-N_i^2\right)^{1/2}+\sum_{j=1}^{i-1}x_j\left[\left(\bar{N}_j^2-N_i^2\right)^{1/2}-\left(\bar{N}_{j+1}^2-N_i^2\right)^{1/2}\right]\right\}, \qquad x_0=0, && (20)\end{aligned}$$

where $\bar{N}_i$ is the average value given by $\bar{N}_i = (N_i+N_{i-1})/2$ for $i=1,2,3,\ldots$ The right hand side of Eq. (17) is equal to

$$\alpha_i = m_i\pi+\phi_a(N(m_i))+\pi/4, \qquad i=1,2,3,\ldots. \tag{21}$$

Next, Eqs. (20) and (21) are combined and solved for the turning point x_i corresponding to a refractive index N_i:

$$x_i = \frac{\alpha_i - k\cdot\sum_{j=1}^{i-1}\left\{x_j\left[\left(\bar{N}_j^2-N_i^2\right)^{1/2}-\left(\bar{N}_{j+1}^2-N_i^2\right)^{1/2}\right]\right\}}{k\left(\bar{N}_i^2-N_i^2\right)^{1/2}} \qquad i=1,2,3,\ldots \tag{22}$$

3. SLAB WAVEGUIDE EXPERIMENTS AND PARAMETER EXTRACTION

An IOG-1 phosphate glass sample was coated by a 500 nm-thick silver layer on both sides of the substrate. Silver ions were driven with an electric field assisted ion exchange into the glass in a temperature controlled oven. At the anode, which acts also as an ion source, the oxidation reaction ($Ag \longrightarrow Ag^+ + e^-$) takes place. The reduction of Na^+ ions occurs at the cathode side. Ion exchange was performed at temperature of 90°C with a voltage of 200 V applied over a 1.5 mm thick substrate. During the process, the silver ion current and the temperature were detected with a multimeter and a thermocouple. After ion exchange, the remnants of the silver film were removed in NH_4OH/H_2O_2 wet etch. The effective indices of the modes propagating in a slab waveguide were then measured by prism coupling. The refractive index profile was constructed according to Chiang's recursive IWKB algorithm described in Section 2.2. Thereafter, Ag^+-ion concentration profile was simulated by Crank-Nicolson method (Section 2.1) by varying the self-diffusion coeffient (D) and the ratio of the self-diffusion coefficients of Ag^+ and Na^+ ions (M) until convergence with the refractive index profile was achieved. It was concluded that the self-diffusion coefficient of Ag^+ ions and the ratio of the self-diffusion coefficients of Ag^+ and Na^+ ions in IOG-1 glass are approximately 5×10^{-18} m^2/s and 0.7 at process conditions used to fabricate two-dimensional waveguides (T = 95°C, U = 200 V).

Ion exchange was followed by annealing at 230°C for 90 min during which the silver ions driven into the glass diffuse deeper to the glass. The self-diffusion coefficient of Ag^+ ions and the ratio of the self-diffusion coefficients of Ag^+ and Na^+ ions were estimated in a similar manner as described above but this time with a zero current $\mathbf{J}_0$ in Eq. 1, since no electric field was applied during the thermal postbake. The diffusion coefficient obtained in this way was approximately 2×10^{-16} m^2/s (diffusion coefficient 3×10^{-16} m^2/s giving an equally good fit) and the ratio of the self-diffusion coefficients of Ag^+ and Na^+ ions ratio was equal to 0.7. The maximum index change produced by replacing Na^+ ions by Ag^+ ions was estimated to be 0.074 and 0.075 at 1535 nm and 980 nm wavelengths, respectively.

4. CHANNEL WAVEGUIDE RESULTS

Using the above estimates for the self-diffusion coefficients, the ratio of the self-diffusion coefficients of Ag^+ and Na^+ ions, and the maximum refractive index change, waveguide mode profiles were theoretically calculated by finite difference time method using a software developed earlier in our group. The calculated and measured mode profiles are presented in Fig. 1 for mask opening width of 3 μm at signal (1535 nm) wavelength. The corresponding calculated and measured mode profiles at pump (980 nm) wavelength are shown in Fig. 2. Measured mode profiles appear to have a slightly elliptic shape with increasing ellipticity as a function of a mask opening width while the theoretical mode profiles show the smallest ellipticity for the waveguide with a mask opening width of 3 μm at signal wavelength. Other theoretically modeled waveguides show increasing ellipticity with a mask opening width. Here, ellipticity is defined as

$$e = \sqrt{\frac{a^2 - b^2}{a^2}}, \tag{23}$$

where a is the major semiaxis and b is the minor semiaxis. Zero ellipticity indicates that the mode width and height are equal. It does not mean, however, that the mode is circular since ion-exchanged waveguide modes are typically asymmetric with regards to the horizontal axis. Both annealing and burial reduce this asymmetry. Theoretically modeled and experimentally measured mode profile dimensions defined at $\frac{1}{e^2}$-intensity point, and ellipticities are given in Tables 1 and 2 for the signal and pump wavelengths, respectively.

5. DISCUSSION

Comparison between the experimental and theoretical results presented in Tables 1 and 2 shows that the self-diffusion coefficient of 2×10^{-16} m^2/s at postbake temperature provides better agreement with the measured data only for the waveguide fabricated with the narrowest mask opening width of 2 μm while for the rest of the mask opening widths the self-diffusion coefficient of 3×10^{-16} m^2/s produces better agreement with the measured mode profiles. It can be also observed that the theoretically calculated mode profile dimensions for the narrowest mask opening width are larger than those for the wider mask opening widths (at 1535 nm). We believe that this results from the fact that the waveguide with the narrowest mask opening width (2 μm) has the

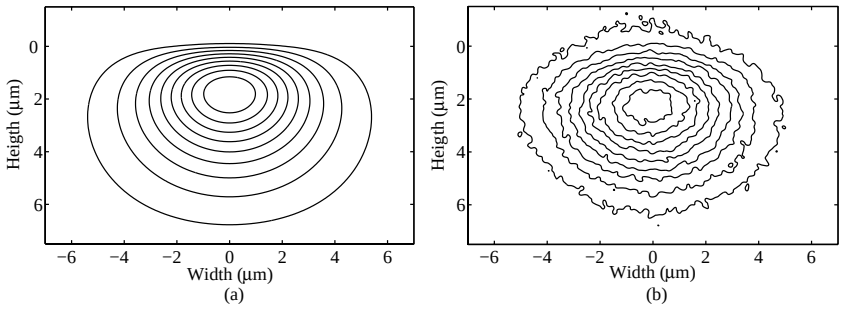

Figure 1. Theoretical (a) and measured (b) mode profiles at signal (1535 nm) wavelength. Waveguide mask opening width is equal to 3 μm, and at postbake temperature a value of 3×10^{-16} m^2/s for self-diffusion coefficient has been used. The intensity difference between the isocontours is 10% of maximum intensity.

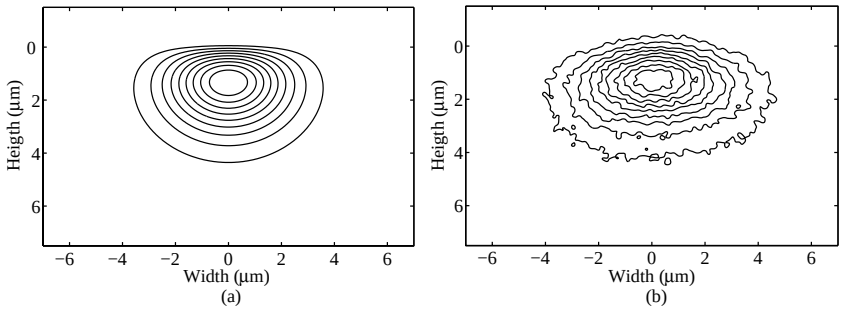

Figure 2. Theoretical (a) and measured (b) mode profiles at pump (980 nm) wavelength. Waveguide mask opening width is equal to 3 μm, and at postbake temperature a value of 3×10^{-16} m^2/s for self-diffusion coefficient has been used. The intensity difference between the isocontours is 10% of maximum intensity.

lowest amount of Ag^+ ions, therefore producing the weakest mode confinement, and furthermore, a relatively large mode size. The modes propagating in other waveguides are more confined which results in a smaller mode profile dimensions. The discrepancies between the theoretically modeled and the measured mode profiles can be explained by the inaccuracies in the lithography process, especially in the case of the mask opening width of 2 μm. At signal wavelength the waveguides with mask opening widths of 2 μm and 3 μm are singlemode while the rest of the waveguides are multimode. At pump wavelength, all the waveguides are multimode. The larger measured mode dimensions in lateral direction compared with the theoretical mode profiles at pump wavelength can be explained by the difficulty to couple light exclusively to the fundamental propagating mode. Calibrations with a standard singlemode fiber (SMF28) at 1550 nm wavelength revealed that the IR-camera itself used in the mode profile measurements is accurate.

Table 1. Mode profile dimensions at different mask opening widths at wavelength of 1535 nm.

Mask opening width [μm]	D [m^2/s]	Width [μm]	Heigth [μm]	Ellipticity
2	measured	8.9	6.4	0.69
2	2×10^{-16}	9.8	6.8	0.73
2	3×10^{-16}	11.0	7.0	0.77
3	measured	9.1	6.3	0.72
3	2×10^{-16}	8.0	5.7	0.70
3	3×10^{-16}	9.6	6.4	0.75
4	measured	8.0	5.4	0.74
4	2×10^{-16}	8.3	5.2	0.78
4	3×10^{-16}	9.1	5.8	0.77
5	measured	9.7	5.7	0.81
5	2×10^{-16}	8.4	4.9	0.81
5	3×10^{-16}	9.0	5.4	0.80

Table 2. Mode profile dimensions at different mask opening widths at (pump) wavelength of 980 nm.

Mask opening width [μm]	D [m^2/s]	Width [μm]	Heigth [μm]	Ellipticity
2	measured	5.9	3.8	0.76
2	2×10^{-16}	6.1	4.0	0.75
2	3×10^{-16}	7.0	4.7	0.74
3	measured	7.7	4.1	0.85
3	2×10^{-16}	5.0	3.5	0.78
3	3×10^{-16}	6.6	4.1	0.78
4	measured	7.7	3.9	0.86
4	2×10^{-16}	6.0	3.4	0.82
4	3×10^{-16}	6.5	3.7	0.82
5	measured	8.9	4.0	0.89
5	2×10^{-16}	6.3	3.3	0.85
5	3×10^{-16}	6.7	3.7	0.83

6. CONCLUSIONS

In this work, we have studied in detail ion exchange and postbake processes used to fabricate single-mode channel waveguides into IOG-1 phosphate glass. Diffusion parameters and the maximum refracive index increase due to the ion exchange were determined. It was concluded that the self-diffusion coefficient is approximately 5×10^{-18} m^2/s at the ion exchange temperature of 90°C and increases to about 3×10^{-16} m^2/s at the postbake temperature of 230°C while the ratio of the self-diffusion coefficients of Ag^+ and Na^+ ions is approximately 0.7 at

both temperatures. Theoretically calculated mode profile dimensions are in good agreement with the measured mode profile dimensions. Knowledge of the self diffusion constant and the ratio of the self-diffusion coefficients of Ag^+ and Na^+ ions has importance in the design of new waveguide components in IOG-1 phosphate glass.

ACKNOWLEDGEMENTS

S. Yliniemi would like to thank the Academy of Finland and Magnus Ehrnrooth's foundation for financial support.

REFERENCES

1. P. Madasamy, G. N. Conti, P. Pöyhönen, M. M. Morrell, D. F. Geraghty, S. Honkanen, and N. Peyghambarian, "Waveguide distributed Bragg reflector laser arrays in erbium doped glass made by dry Ag film ion exchange," *Opt. Eng.* **41**, pp. 1084–1086, 2002.
2. S. Blaize, L. Bastard, C. Cassagnètes, and J. E. Broquin, "Multiwavelengths DFB waveguide laser arrays in Yb-Er codoped phosphate glass substrate," *IEEE Photon. Technol. Lett.* **15**, pp. 516–518, 2003.
3. S. Yliniemi, J. Albert, Q. Wang, and S. Honkanen, "UV-exposed Bragg gratings for laser applications in silver-sodium ion-exchanged phosphate glass waveguides," *Opt. Exp.* **14**, pp. 2898–2903, 2006.
4. D. L. Veasey, D. S. Funk, P. M. Peters, N. A. Sanford, G. E. Obarski, N. Fontaine, M. Young, A. P. Peskin, W.-C. L. S. N. Houde-Walter, and J. S. Hayden, "Yb/Er-codoped and Yb-doped waveguide lasers in phosphate glass," *J. Non-Cryst. Solids* **263&264**, pp. 369–381, 2000.
5. S. Honkanen and A. Tervonen, "Experimental analysis of Ag^+-Na^+ ion exchange in glass with Ag film ion sources for planar optical waveguide fabrication," *J. Appl. Phys.* **63**, pp. 634–639, 1988.
6. R. Terai and R. Hayami, "Ionic diffusion in glasses," *J. Non-Cryst. Solids* **18**, p. 217264, 1975.
7. A. Tervonen, "A general model for fabrication processes of channel waveguides by ion exchange," *J. Appl. Phys.* **67**, pp. 2746–2752, 1990.
8. A. Tervonen, S. Honkanen, and M. Leppihalme, "Control of ion-exchanged waveguide profiles with Ag thin film sources," *J. Appl. Phys.* **62**, pp. 759–763, 1987.
9. A. Tervonen, "Theoretical analysis of ion-exchanged glass waveguides," in *Introduction to Glass Integrated Optics*, S. I. Najafi, ed., pp. 73–105, Artech House, Boston, 1992.
10. C. F. Gerald and P. O. Wheatley, *Applied Numerical Analysis*, Addison-Wesley Publishing Company, Reading, USA, 1994 (fifth edition).
11. J. H. Ferziger, *Numerical Methods for Engineering Application*, John Wiley & Sons, New York, USA, 1981.
12. E. Merzbacher, *Quantum Mechanics*, John Wiley & Sons, Inc., New York, USA, 1998 (third edition).
13. R. L. Liboff, *Introductory Quantum Mechanics*, Addison-Wesley Publishing Company, Inc., Reading, USA, 1992 (second edition).
14. C. R. Pollock, *Fundamentals of Optoelectronics*, Ceramic Book & Literature, New Delhi, India, 2003 (first edition).
15. M. Born and E. Wolf, *Principles of Optics*, Cambridge University Press, Cambridge, United Kingdom, 1998 (sixth (corrected) edition).
16. K. S. Chiang, "Construction of refractive-index profiles of planar dielectric waveguides from the distribution of effective indexes," *J. Lightwave Technol.* **LT-3**, pp. 385–391, 1985.